Research Article Vol. 29, No. 14 / 5 July 2021 / Optics Express 22567
Optics EXPRESS

Photoacoustic laser streaming with non-plasmonic metal ion implantation in transparent substrates

XIN AI,[1,2,7] FENG LIN,[1,2,7,8] TIAN TONG,[3] DI CHEN,[4] SHUAI YUE,[1,3,5] MOHAMMADJAVAD MOHEBINIA,[6] JAYAHANSA NAPAGODA,[4] YUNAO QIU,[1,2,3] XIN TONG,[1,2] PENG YU,[1,2] WEI-KAN CHU,[4] JIMING BAO,[3,4,6,9] AND ZHIMING WANG[1,2,10]

[1] *Institute of Fundamental and Frontier Sciences, University of Electronic Science and Technology of China, Chengdu, Sichuan 610054, China*
[2] *Yangtze Delta Region Institute (Huzhou), University of Electronic Science and Technology of China, Huzhou 313001, China*
[3] *Department of Electrical and Computer Engineering, University of Houston, Houston, TX 77204, USA*
[4] *Department of Physics and Texas Center for Superconductivity, University of Houston, Houston, TX 77204, USA*
[5] *National Center for Nanoscience and Technology, Beijing 100190, China*
[6] *Materials Science and Engineering, University of Houston, Houston, TX 77204, USA*
[7] *These authors contributed equally to this work*
[8] *fenglin0928@hotmail.com*
[9] *jbao@uh.edu*
[10] *zhmwang@uestc.edu.cn*

Abstract: Photoacoustic laser streaming provides a versatile technique to manipulate liquids and their suspended objects with light. However, only gold was used in the initial demonstrations. In this work, we first demonstrate that laser streaming can be achieved with common non-plasmonic metals such as Fe and W by their ion implantations in transparent substrates. We then investigate the effects of ion dose, substrate material and thickness on the strength and duration of streaming. Finally, we vary laser pulse width, repetition rate and power to understand the observed threshold power for laser streaming. It is found that substrate thickness has a negligible effect on laser streaming down to 0.1 mm, glass and quartz produce much stronger streaming than sapphire because of their smaller thermal conductivity, while quartz exhibits the longest durability than glass and sapphire under the same laser intensity. Compared with Au, Fe and W with higher melting points show a longer lifetime although they require a higher laser intensity to achieve a similar speed of streaming. To generate a continuous laser streaming, the laser must have a minimum pulse repetition rate of 10 Hz and meet the minimum pulse width and energy to generate a transient vapor layer. This vapor layer enhances the generation of ultrasound waves, which are required for observable fluid jets. Principles of laser streaming and temperature simulation are used to explain these observations, and our study paves the way for further materials engineering and device design for strong and durable laser streaming.

1. Introduction

The ability to manipulate or drive liquid is the basic requirement of many fluid-related applications such as microfluidics [1,2], chemical microreactors [3], and bioscience systems [4,5]. Optical techniques of fluid control can offer more advantages over conventional mechanical methods with non-contact, precise temporal-spatial liquid actuation and low fabrication cost [1]. However, most optical techniques that utilize effects such as optical radiation pressure [6], thermocapillarity [4,7], photophoresis [8], and optoelectrowetting [9] suffer from a weak liquid-driving force. Recently

#430025 https://doi.org/10.1364/OE.430025
Journal © 2021 Received 3 May 2021; revised 6 Jun 2021; accepted 8 Jun 2021; published 1 Jul 2021

discovered photoacoustic laser streaming overcomes this limitation by combining photoacoustic effect with strong acoustic streaming, and subsequent demonstration of photoacoustic laser pumps by Au ion implantation in quartz has allowed people to generate flow from any point in a large area quartz slide [10–12]. These pioneer works and other related developments have established the principle of laser streaming and paved the way for its novel applications [13–17], however, many open questions remain. For example, is Au necessary for laser streaming? Besides quartz and glass substrates, can we use other transparent materials? The answers to these questions not only help us to understand the complicated process of laser streaming involving optical, electronic, thermal and mechanical interactions, but also facilitate the design and development of higher performance laser steaming pumps.

In this work, we will first explore the ion implantation of the most common metal iron (Fe) in quartz slides for photoacoustic laser streaming. Tungsten (W) is then chosen for comparison with Fe and Au. Glass and sapphire are selected for ion implantation as two closely related transparent materials to quartz. Besides metals and substrates, we also systematically vary the ion implantation dose and substrate thickness and investigate their effects on the performance of laser streaming in terms of flow speed and duration. Finally, these effects and observations will be analyzed and explained based on the principle of laser streaming and temperature simulation.

2. Experimental setup

Laser streaming experiments were performed in a similar setup to our previous research as shown in Fig. 1(a) [10]. Here we used a more common 532-nm laser instead of 527-nm laser while keeping the same pulse width of 150 ns and the same 1 kHz repetition frequency. A lens with a shorter focal length of 5 cm was used to focus laser on the ion implanted substrates to generate streams. Flow speed and patterns were observed and recorded by a high-speed camera through a zoom lens (Shenzhen Fangte: FT-U3F500). A thermal camera (FLIR E8-XT) was used to measure the temperature distribution of laser focused substrate in air. A combination of shadowgraph and stroboscopic photography was used to detect transient vapor, and a second and delayed laser pulse was used as a strobe light.

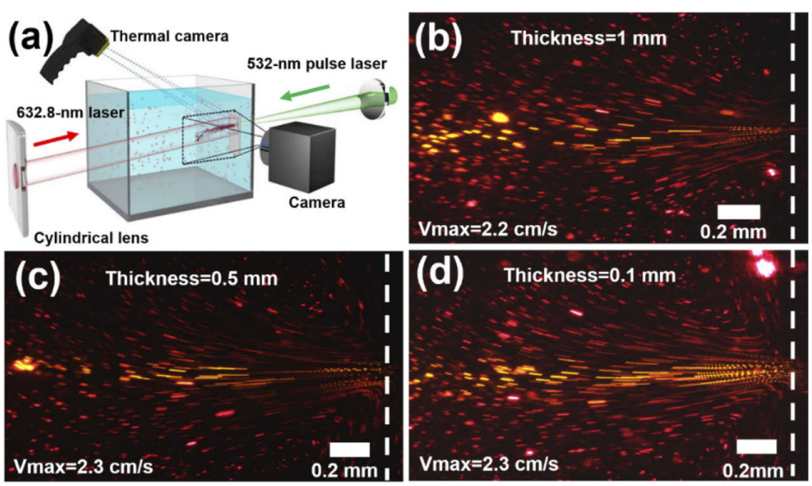

Fig. 1. Photoacoustic laser streaming from Fe ion implanted quartz slides. (a) Schematic of experimental setup. Thermal camera images were obtained in air without water. (b-d) Snapshots of streaming from three quartz slides with thickness of (b) 1 mm, (c) 0.5 mm and (d) 0.1 mm. The implantation dose is $2{\times}10^{17}/cm^2$ and the incident laser power is 30 mW.

3. Results and discussion

In the discovery and initial demonstration of laser streaming, Au was chosen because Au nanoparticles are widely used in photoacoustic imaging as contrast agent and display a strong optical absorption at the excitation laser wavelength due to surface plasmon resonance [18–20]. But this unique plasmonic property of Au nanoparticles also limits the selection of laser and many potential applications of laser streaming [21,22]. To demonstrate the laser streaming with non-plasmonic metals and find the effect of surface plasmon resonance on laser streaming, we chose Fe, a most common and low-cost metal. We used 1-mm thick quartz substrate as before and ion implanted the substrate with Fe to a dose of $2{\times}10^{17}/cm^2$ at 55 kV. Surprisingly, a jet was immediately generated from the Fe implanted quartz substrate immediately after turn-on of the laser. Figure 1(b) shows the stream line of the jet, it can be seen that its flow pattern and flow velocity are comparable with those from Au implanted quartz [10]. This finding proves that Au is not the only material for laser streaming, many other metals and different lasers can be used to generate photoacoustic laser streaming.

Since the ultrasound wave for laser streaming is launched from the quartz substrate, its generation should be affected by the mechanical property of the substrate. In fact, it is well known that a slab (slide) of quartz crystal is an excellent mechanical oscillator because it possesses a spectrum of fundamental vibration frequency determined by its geometry and size. To investigate the substrate effect, we chose quartz slides with three thicknesses at 1, 0.5 and 0.1 mm, and implanted them with Fe ions to the same dose. Figures 1(b)–1(d) show the snapshots of jet streams under the excitation of 30 mW laser. Despite a large difference in the thickness, three jets have very close flow velocity. This observation indicates that the photoacoustic wave from the laser focus spot is not strongly coupled to the whole body of the quartz slide. In the remaining experiments, all the samples were prepared on substrate with thickness of 1 mm.

Besides the thickness, the type of substrate material is certainly another and even more important consideration for photoacoustic wave because of very different mechanical and thermal properties. Although both quartz and glass (amorphous quartz) were used to demonstrate laser streaming because they are the most common laboratory materials as cover slides and cuvettes, only quartz was used for ion implantation [10]. For a better comparison of substrate with vastly different mechanical and thermal properties, we chose sapphire in comparison with quartz and glass. We implanted the same dose of Au ions in these three types of substrates and compared laser streaming under the same laser power of 20 mW. The snapshots of liquid flows in Figs. 2(a)–2(c) reveal a huge difference between sapphire and quartz/glass: the streaming from sapphire is almost invisible while glass substrate exhibits the highest initial flow speed of 3.1 cm/s. Sapphire is mechanically stronger and has a much higher melting point than quartz and glass, so it is expected to produce a stronger acoustic wave and stronger streaming.

To investigate the cause of much weaker streaming from sapphire, we turned our attention to their differences in thermal properties. The insets in Fig. 2(d) show the thermal images of steady-state temperature distribution of the three substrates from the back side in air. It should be noted that due to slow response of the camera, thermal images here are averaged temperature distribution instead of a transient temperature gradient around the incident point of laser. Nevertheless, the difference between three substrates is clear: sapphire (glass) has the lowest (highest) local temperature at the laser focus spot, respectively. This difference comes from the difference in their thermal conductivity: sapphire (glass) has the highest (lowest) thermal conductivity of 34 W/m·K and 1 W/m·K, respectively. A higher substrate thermal conductivity provides faster heat dissipation, resulting in a lower local temperature [23]. This understanding can be further supported by our heat transfer simulation with Simulia Abaqus (details shown in Supplement 1). Figure 2(d) shows the time evolution of the temperature of laser spot in Au-implanted glass, quartz and sapphire. A larger effect of substrate thermal conductivity on the transient temperature than the steady-state temperature can be seen, here the evaporation of

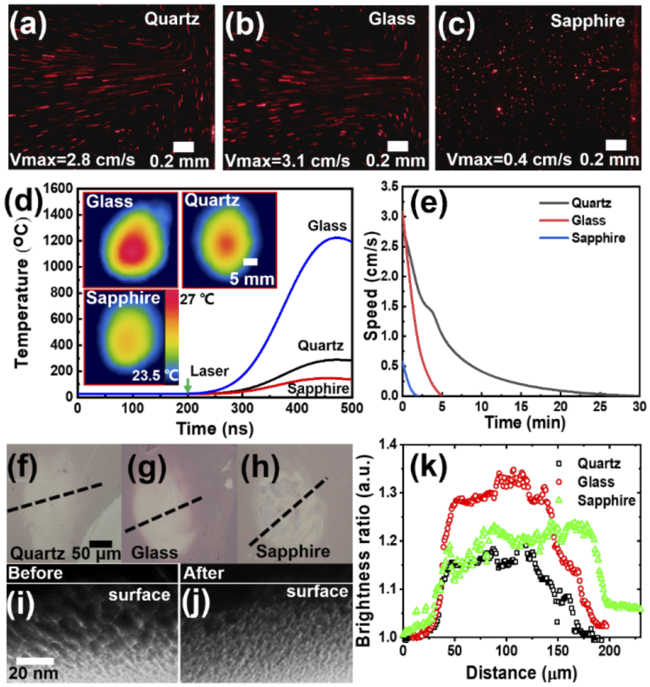

Fig. 2. Laser streaming with different types of substrates. (a-c) Snapshots of streaming from Au implanted (a) quartz, (b) glass and (c) sapphire under the excitation of 20 mW laser. (d) Simulated temperature evolution of laser spot in Au-implanted glass, quartz and sapphire plates. Insets are steady-state thermal images of the three samples in air. (e) Decay of flow speed with the three substrates. (f-h) Optical transmission images of (f) quartz, (g) glass and (h) sapphire plates after 2 minutes of laser irradiation. (i-j) The cross-section TEM images of the Au-implanted glass before and after laser heating. (k) Relative brightness ratio between irradiated region and surrounding area along the dotted line in (f)-(h). The power of laser was 20 mW.

water above its boiling point is neglected. These observations suggest that local temperature is important for the generation of photoacoustic wave.

Streaming speed is not the only consideration in the selection of substrate, durability is also important for practical devices. Using the existing three Au-implanted substrates, we then monitored the streaming over time under the same laser power. The results from Fig. 2(e) show that although streaming from all three substrates decreases significantly, streaming from quartz lasts much longer than that from sapphire and glass. The decreased jet speed must be due to laser induced damage to the ion implanted Au or substrates, and such damages are ubiquitous and have been well reported [24,25]. A quick visual inspection in Figs. 2(f)–2(h) confirms the damages and reveals increased optical transmission through laser irradiated spots due to the loss of implanted Au. The cross-section TEM images of Au-implanted glass in Figs. 2(i)–2(j) indicate that the implanted Au breaks into very small particles, and less Au remains in the original position after laser irradiation. A quantitative analysis of relative brightness between irradiated and surrounding region in Fig. 2(i) further reveals that glass suffers from more loss of implanted Au ions, which explain the faster decrease of streaming from glass substrate than quartz. In summary, quartz is a better choice than glass and sapphire for strong and long-lasting streaming.

A convenient way to generate a strong jet is to increase implantation dose because a higher dose will induce a stronger optical absorption. However, different materials might have different

Optics EXPRESS

optimal doses and different effect of dose on the streaming. To obtain a rough comparison, we chose two doses of 5×10^{16}/cm^2 and 1×10^{17}/cm^2 for Fe and Au implantations. Figure 3(a) shows optical images of Au- and Fe-implanted quartz plates. The Fe and Au implantations can be quickly distinguished by a reddish color of Au and a dark color of Fe. This difference can also be seen from their optical transmission in Fig. 3(b), where the Au-implanted plate shows an obvious transmission dip in short-wavelength because of surface plasmon resonance around 532 nm [26]. Because of higher optical absorption of Au than Fe, Au implanted quartz slides produce stronger jets, as shown in Figs. 3(c)–3(f), however, when the dose doubles, the speed of jet from Au implantation only increases slightly, while the jet speed increases more than double for Fe implantation. Therefore, higher incident laser power or higher dosage is required for Fe in order to achieve the same jet speed as Au implantation [27].

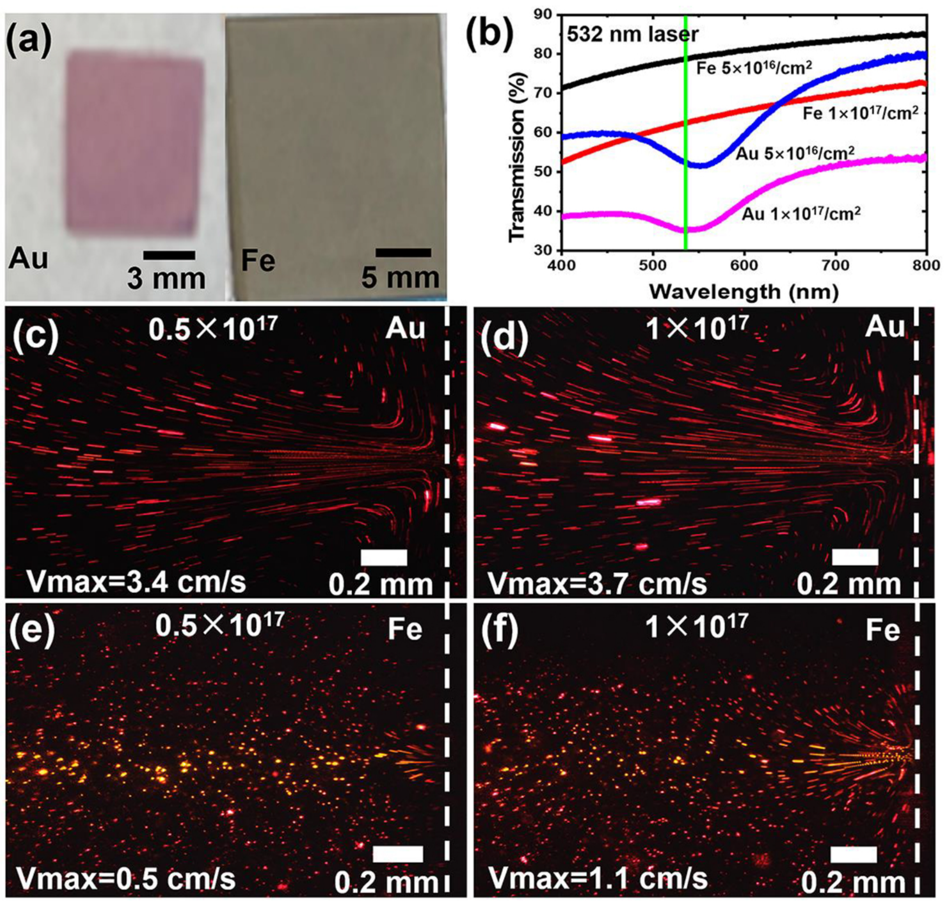

Fig. 3. Laser streaming of Au and Fe implanted quartz substrates with different concentrations. (a) Optical images and (b) transmission spectra of Au and Fe implanted quartz plates. (c-f) Snapshots of jets from (c-d) Au and (e-f) Fe implanted quartz substrates. The incident laser power was 30 mW.

To better compare efficiency of laser streaming with different metals, we adjusted implantation doses such that a similar optical absorption was reached for different metals. We prepared two sets of metals with Fe vs. Au as one group whereas Fe vs. W as the other group. Figures 4(a)–4(b) show transmission spectra of four implanted quartz substrates, where the Fe/Au group has an

Optics EXPRESS

absorption of ~50% and the absorption of Fe/W group is ~24%. Figures 4(c)–4(d) summarize evolutions of streaming from the four samples. It can be seen that the Au is much more efficient than Fe in laser streaming under the same optical absorption and excitation, but Fe is more stable than Au. A much higher laser power is needed for Fe implanted substrate than Au implanted quartz to generate flow at the same speed. Between Fe and W, Fe is more efficient, but W has slightly more stable than Fe.

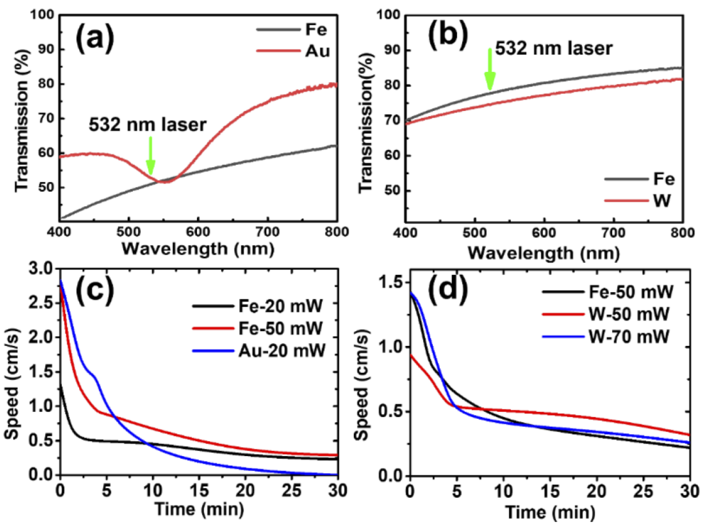

Fig. 4. Comparison of laser streaming from quartz substrates implanted by Au, Fe and W. (a) Optical transmission spectra of quartz substrates implanted by Fe and Au. (b) Optical transmission spectra of quartz substrates implanted by Fe and W. (c) Evolution of speed of jets from Fe and Au implanted quartz substrates in (a). (d) Evolution of speed of jets from Fe and W implanted quartz substrates in (b).

The demonstration of laser streaming with non-plasmonic metal ion implantation and the most of above observations can be understood from the fundamental principle of photoacoustic laser streaming. Although laser streaming is a combination of photoacoustic effect [13,15,16] and acoustic streaming [14], photoacoustic effect takes place before acoustic streaming and determines the strength of streaming. Because photoacoustic effect is a photothermal effect, as long as laser pulses can be absorbed and converted to heat, photoacoustic wave will be generated to drive the liquid, this is why both Fe and W work like Au, and other metals and non-metals are also expected to work [27,28]. On the other hand, there does not exist a general microscopic picture of the generation of ultrasound through the photothermal effect, and each case can be different depending on detailed experimental conditions. Taking Au nanoparticles suspended in water as an example, ultrasound can be generated either by thermal expansion of Au nanoparticles themselves, or by thermal expansion of the surrounding water, or by transient water vapor around nanoparticles [22,29]. In most cases, all these factors will contribute to the generation of ultrasound.

Besides implantation and substrate materials, the laser itself is certainly critical for photoacoustic laser streaming; in particular, our earlier work observed that a minimum incident power was required [11]. Below such threshold, the streaming suddenly disappeared. A threshold power is also observed with the 532-nm laser and ion implanted samples in this study. Figure 5(a) shows the threshold power of Au and Fe samples with different implantation concentrations; here the threshold power is calculated as the absorbed power based on the absorption coefficient and incident power because the absorbed power will actually drive the photoacoustic waves. The

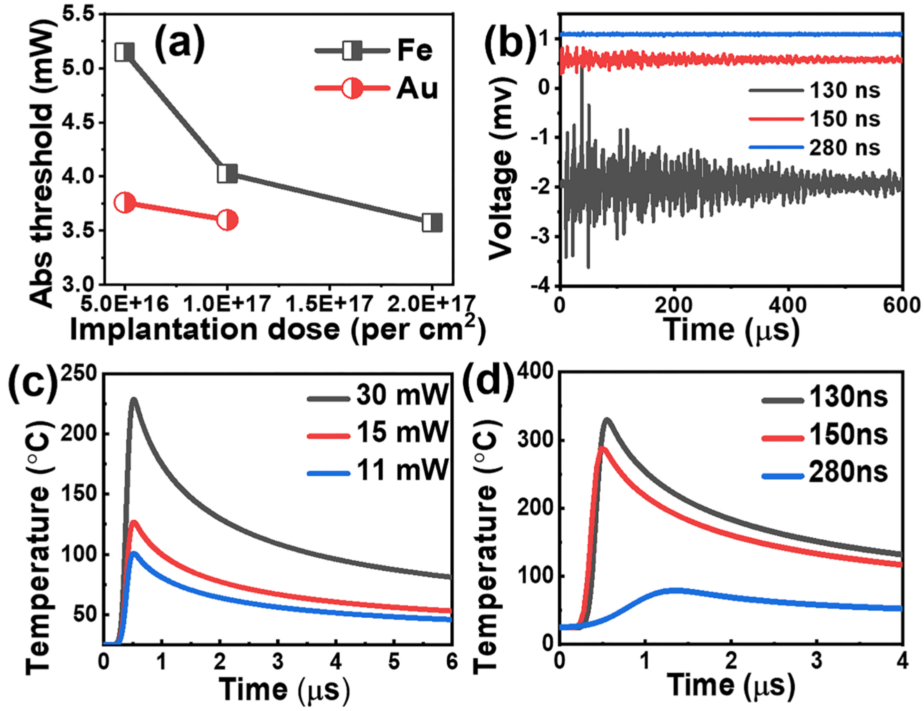

Fig. 5. The effect of laser parameters on photoacoustic laser streaming. (a) Absorbed threshold power for laser streaming using quartz plates with different implantation doses. (b) Acoustic signals generated by 527-nm pulses with different pulse width. (c) Simulated temperature evolution of laser spot in the Au-implanted quartz as in Fig. 4(a) under the 532-nm laser with different incident powers. (d) Simulated temperature evolution for the experiment in (b).

pulse width is also an important parameter, a shorter pulse will result in a higher frequency of the generated acoustic wave [30,31]. To explore its effect on the laser streaming, we vary the pulse width of 527 nm laser from 110 ns to 280 ns while keeping the energy of each pulse fixed. Figure 5(b) shows that with increasing pulse width, the acoustic signals decrease dramatically, and at 280 ns it become too weak to be detected and laser streaming disappears completely [10,30,31]. To understand the effect of power and pulse width, we also performed photothermal simulation. Figure 5(c) reveals that the peak temperature of sample surface decreases quickly as power is reduced and drops below the water boiling point at 11 mW. The same happens with the pulse width; Fig. 5(d) shows that the temperature drops far below 100 ℃ when the pulse width increases to 280 ns. These results indicate that the peak intensity is important for laser streaming. High peak intensity can be satisfied with pulsed lasers [33,34]. A simple intensity modulation of a CW laser by a mechanical chopper or an acousto-optic modulator will not produce high intensity laser pulses for laser streaming despite a shorter pulse width [32–34].

The temperature simulations and the observed threshold power and pulse width suggest the generation of transient vapor in the photothermal process of laser streaming. Transient vapor was proposed in our first work to understand the threshold power [11], but was not confirmed in our second work because no obvious bubble was observed [10]. To resolve this discrepancy and obtain a better picture of ultrasound generation mechanism, we employ a high-speed shadowgraph technique to detect any possible vapor or bubble [35,36]. Figure 6(a) shows the schematic of experimental setup. A 527-nm pump laser is used to generate streaming as usual; a second

Optics EXPRESS

527-nm laser is used as a strobe light to illuminate the flow in the front of the camera to create an optical shadow. The pulse from the second laser is synchronized with the pump pulse using a delay generator. Because both the delay and pulse width can be tuned on the nanosecond scale, this high-speed shadowgraph offers a sub-microsecond time resolution, and it enables us to capture the transient vapor. Figure 6(b) shows the moment the pump pulse strikes the Au-implanted quartz, Fig. 6(c) shows the time when vapor is fully developed after 6 µs. Note that the vapor forms a thin layer on the quartz surface and doesn't develop into a full and detached bubble as typically observed [37–40]. Compared to the large volume change of water vapor, the thermal expansions of implanted metals and transparent substrates can be neglected [41,42]; this is why transient vapor can enhance photoacoustic effect so much that it becomes a necessary condition for laser streaming. Its thin layer has also avoided creating complicated flows or disturbances that would be induced by larger sized bubbles.

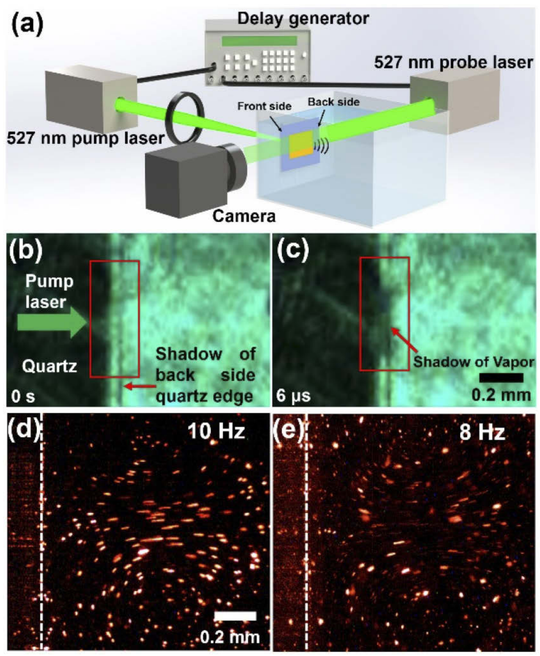

Fig. 6. Laser-induced vapor film. (a) Experimental setup of high-speed shadowgraph technique. (b-c) Shadowgraphs at delay time of 0 and 6 µs. (d-e) Snapshots of jets when the laser repetition rate is (d) 10 Hz and (e) 8 Hz.

The observation of transient vapor and photothermal simulation help us to qualitatively understand other observations. Since a higher local temperature will generate more vapor and subsequently a stronger ultrasound wave, the thickness of a substrate should have no effect on laser streaming, while a high thermal conductivity of substrate will greatly reduce laser streaming. Because Au has a much higher thermal conductivity than that of Fe and W, thermal energy can be efficiently transferred to water during laser irradiation, this is why Au is more effective for laser streaming than Fe and W [22,27]. Due to the same reason, the threshold power of Au is lower than that of Fe, samples with a higher implantation dose have a lower threshold power. This is because the highly implanted region will have a higher thermal conductivity due to a higher metallic atom concentration. As for the duration of laser streaming, we believe it is related to the mechanical and thermal properties of implanted metals and substrates, because the decay of streaming is caused by the loss of implanted metals. Specifically, we believe that the lower melting point of Au is responsible for its shorter lifetime compared with Fe and W, and higher melting point and stronger mechanical strength of quartz is responsible for its longer streaming compared to glass. Finally, we want to point out that laser streaming can also be tuned by incident laser power and beam size. The relatively shorter streaming time in this work is due to much tighter laser focusing than before [10,11]. When a lens with longer focal length of 15 centimeters is used, the streaming can easily last for over one hour without significant decay for any metals. Since each jet generated from a single laser pulse can last for about 100 ms according to our previous work [10], a minimum of 10 Hz is required to generate a continuous flow, as can be seen from Figs. 6(d) and 6(e).

4. Conclusion

In summary, we have demonstrated photoacoustic laser streaming using non-plasmonic metals implanted in transparent substrates, we have found that quartz is the best substrate for strong and durable streaming, Au is the best metal for strong streaming, while Fe and W are better for durable streaming. A combination of a metal with high thermal conductivity and a substrate with low thermal conductivity is required to generate a strong streaming, while to achieve long-lasting streaming, metals with higher melting points and substrates with higher melting points and stronger mechanical strength are preferred. The generation of transient vapor is observed by high speed shadowgraph, and it sets the threshold of laser power and pulse width for laser streaming. Since a high local temperature and ultrasound will be created by pulsed laser, damage to materials is inevitable, thus it remains as a challenge to achieve strong and long-lasting streaming, more research is needed to identify new materials and make new device design for practical applications in microfluidics and optofluidics.

Funding. National Natural Science Foundation of China (52002049, 62075034, 62005037); National Science Foundation (CBET-1932734); Welch Foundation (E-1728); Sichuan Province Science and Technology Support Program (No. 2021YFH0054, No. 2020YJ0041); China Postdoctoral Science Foundation 2019M663467.

Disclosures. The authors declare that there are no conflicts of interest related to this article.

Data availability. Data underlying the results presented in this paper are not publicly available at this time but may be obtained from the authors upon reasonable request.

Supplemental document. See Supplement 1 for supporting content.

References

1. D. Baigl, "Photo-actuation of liquids for light-driven microfluidics: state of the art and perspectives," Lab Chip **12**(19), 3637–3653 (2012).
2. H. Ahmed, S. Ramesan, L. Lee, A. R. Rezk, and L. Y. Yeo, "On-Chip Generation of Vortical Flows for Microfluidic Centrifugation," Small **16**(9), 1903605 (2020).
3. D. M. Roberge, B. Zimmermann, F. Rainone, M. Gottsponer, M. Eyholzer, and N. Kockmann, "Microreactor Technology and Continuous Processes in the Fine Chemical and Pharmaceutical Industry: Is the Revolution Underway?" Org. Process Res. Dev. **12**(5), 905–910 (2008).
4. A. Sutton, T. Shirman, J. V. Timonen, G. T. England, P. Kim, M. Kolle, T. Ferrante, L. D. Zarzar, E. Strong, and J. Aizenberg, "Photothermally triggered actuation of hybrid materials as a new platform for in vitro cell manipulation," Nat. Commun. **8**(1), 14700 (2017).
5. Y.-N. Wang and L.-M. Fu, "Micropumps and biomedical applications – A review," Microelectron. Eng. **195**, 121–138 (2018).
6. A. Ashkin, "Acceleration and Trapping of Particles by Radiation Pressure," Phys. Rev. Lett. **24**(4), 156–159 (1970).
7. C. Gao, L. Wang, Y. Lin, J. Li, Y. Liu, X. Li, S. Feng, and Y. Zheng, "Droplets Manipulated on Photothermal Organogel Surfaces," Adv. Funct. Mater. **28** (2018).
8. S. Tehranian, F. Giovane, J. Blum, Y. L. Xu, and B. A. S. Gustafson, "Photophoresis of micrometer-sized particles in the free-molecular regime," Int. J. Heat Mass Transfer **44**(9), 1649–1657 (2001).
9. F. Mugele and J. C. Baret, "Electrowetting: From basics to applications," J. Phys.: Condens. Matter **17**(28), R705–R774 (2005).
10. S. Yue, F. Lin, Q. Zhang, N. Epie, S. Dong, X. Shan, D. Liu, W. K. Chu, Z. Wang, and J. Bao, "Gold-implanted plasmonic quartz plate as a launch pad for laser-driven photoacoustic microfluidic pumps," Proc. Natl. Acad. Sci. U. S. A. **116**(14), 6580–6585 (2019).
11. Y. N. Wang, Q. H. Zhang, Z. A. Zhu, F. Lin, J. D. Deng, G. Ku, S. C. Dong, S. Song, M. K. Alam, D. Liu, Z. M. Wang, and J. M. Bao, "Laser streaming: Turning a laser beam into a flow of liquid," Sci. Adv. **3**(9), e1700555 (2017).

Optics EXPRESS

12. G. Qu, Y. Wang, Z. Zhong, M. Li, M. Zhou, D. Liu, Z. Xu, W. Lin, X. Liu, and J. Han, "Formation mechanism of the nanostructure in laser streaming phenomenon," Opt. Express **28**(21), 30586–30596 (2020).
13. Y. Hou, J.-S. Kim, S. Ashkenazi, S.-W. Huang, L. J. Guo, and M. O'Donnell, "Broadband all-optical ultrasound transducers," Appl. Phys. Lett. **91**(7), 073507 (2007).
14. B. Moudjed, V. Botton, D. Henry, S. Millet, J. P. Garandet, and H. Ben Hadid, "Oscillating acoustic streaming jet," Appl. Phys. Lett. **105**(18), 184102 (2014).
15. B. Zhang, C. Y. Fang, C. C. Chang, R. Peterson, S. Maswadi, R. D. Glickman, H. C. Chang, and J. Y. Ye, "Photoacoustic emission from fluorescent nanodiamonds enhanced with gold nanoparticles," Biomed. Opt. Express **3**(7), 1662 (2012).
16. C. W. Van Neste, L. R. Senesac, and T. Thundat, "Standoff photoacoustic spectroscopy," Appl. Phys. Lett. **92**(23), 234102 (2008).
17. A. Farhadi, G. H. Ho, D. P. Sawyer, R. W. Bourdeau, and M. G. Shapiro, "Ultrasound imaging of gene expression in mammalian cells," Science **365**(6460), 1469–1475 (2019).
18. W. Li and X. Chen, "Gold nanoparticles for photoacoustic imaging," Nanomedicine **10**(2), 299–320 (2015).
19. A. Feis, C. Gellini, P. R. Salvi, and M. Becucci, "Photoacoustic excitation profiles of gold nanoparticles," Photoacoustics **2**(1), 47–53 (2014).
20. L. V. Wang and S. Hu, "Photoacoustic tomography: in vivo imaging from organelles to organs," Science **335**(6075), 1458–1462 (2012).
21. M. Gandolfi, F. Banfi, and C. Glorieux, "Optical wavelength dependence of photoacoustic signal of gold nanofluid," Photoacoustics **20**, 100199 (2020).
22. T. Lee, H. W. Baac, Q. C. Li, and L. J. Guo, "Efficient Photoacoustic Conversion in Optical Nanomaterials and Composites," Adv. Opt. Mater. **6**(24), 1800491 (2018).
23. S. Yue, G. A. Gamage, M. Mohebinia, D. Mayerich, V. Talari, Y. Deng, F. Tian, S. Y. Dai, H. Sun, V. G. Hadjiev, W. Zhang, G. Feng, J. Hu, D. Liu, Z. Wang, Z. Ren, and J. Bao, "Photoluminescence mapping and time-domain thermo-photoluminescence for rapid imaging and measurement of thermal conductivity of boron arsenide," Mater. Today Phys. **13**, 100194 (2020).
24. Y. Chai, M. Zhu, Z. Bai, K. Yi, H. Wang, Y. Cui, and J. Shao, "Impact of substrate pits on laser-induced damage performance of 1064-nm high-reflective coatings," Opt. Lett. **40**(7), 1330–1333 (2015).
25. J. Krüger, D. Dufft, R. Koter, and A. Hertwig, "Femtosecond laser-induced damage of gold films," Appl. Surf. Sci. **253**(19), 7815–7819 (2007).
26. A. O. Govorov and H. H. Richardson, "Generating heat with metal nanoparticles," Nano Today **2**(1), 30–38 (2007).
27. T. Lee and L. J. Guo, "Highly Efficient Photoacoustic Conversion by Facilitated Heat Transfer in Ultrathin Metal Film Sandwiched by Polymer Layers," Adv. Opt. Mater. **5**(2), 1600421 (2017).
28. A. D. Silva, C. A. Henriques, D. V. Malva, M. J. F. Calvete, M. M. Pereira, C. Serpa, and L. G. Arnaut, "Photoacoustic generation of intense and broadband ultrasound pulses with functionalized carbon nanotubes," Nanoscale **12**(40), 20831–20839 (2020).
29. J. M. Fernandez-Pradas, C. Florian, F. Caballero-Lucas, P. Sopena, J. L. Morenza, and P. Serra, "Laser-induced forward transfer: Propelling liquids with light," Appl. Surf. Sci. **418**, 559–564 (2017).
30. Y. Hou, J.-S. Kim, S. Ashkenazi, S.-W. Huang, L. J. Guo, and M. O'Donnell, "Broadband all-optical ultrasound transducers," Appl. Phys. Lett., **91** (2007).
31. Y. Hou, S. Ashkenazi, S. W. Huang, and M. O'Donnell, "Improvements in optical generation of high-frequency ultrasound," IEEE Trans. Ultrason. Ferroelectr. Freq. Control. **54**(3), 682–686 (2007).
32. K. Maslov and L. V. Wang, "Photoacoustic imaging of biological tissue with intensity-modulated continuous-wave laser," J. Biomed. Opt. **13**(2), 024006 (2008).
33. T. J. Allen and P. C. Beard, "High power visible light emitting diodes as pulsed excitation sources for biomedical photoacoustics," Biomed. Opt. Express **7**(4), 1260–1270 (2016).
34. K. Daoudi, P. J. van den Berg, O. Rabot, A. Kohl, S. Tisserand, P. Brands, and W. Steenbergen, "Handheld probe integrating laser diode and ultrasound transducer array for ultrasound/photoacoustic dual modality imaging," Opt. Express **22**(21), 26365–26374 (2014).
35. V. M. Chudnovskii, A. A. Levin, V. I. Yusupov, M. A. Guzev, and A. A. Chernov, "The formation of a cumulative jet during the collapse of a vapor bubble in a subcooled liquid formed as a result of laser heating," Int. J. Heat. Mass. Tran., **150** (2020).
36. J. Long, M. Eliceiri, Z. Vangelatos, Y. Rho, L. Wang, Z. Su, X. Xie, Y. Zhang, and C. P. Grigoropoulos, "Early dynamics of cavitation bubbles generated during ns laser ablation of submerged targets," Opt. Express **28**(10), 14300–14309 (2020).
37. H. Ju, R. A. Roy, and T. W. Murray, "Gold nanoparticle targeted photoacoustic cavitation for potential deep tissue imaging and therapy," Biomed. Opt. Express **4**(1), 66–76 (2013).
38. Y. E. Tian, N. A. N. Wu, K. A. I. Sun, X. Zou, and X. Wang, "Numerical Simulation of Fiber-Optic Photoacoustic Generator Using Nanocomposite Material," J. Theor. Comput. Acoust., **21** (2013).
39. V. K. Pustovalov, A. S. Smetannikov, and V. P. Zharov, "Photothermal and accompanied phenomena of selective nanophotothermolysis with gold nanoparticles and laser pulses," Laser Phys. Lett. **5**(11), 775–792 (2008).
40. J. Li, F. Zhao, Y. Deng, D. Liu, C. H. Chen, and W. C. Shih, "Photothermal generation of programmable microbubble array on nanoporous gold disks," Opt. Express **26**(13), 16893–16902 (2018).

Optics EXPRESS

41. M. Mohammadzadeh, S. R. Gonzalez-Avila, K. Liu, Q. J. Wang, and C.-D. Ohl, "Synthetic jet generation by high-frequency cavitation," J. Fluid Mech. **823**, R3 (2017).
42. D. Obreschkow, M. Tinguely, N. Dorsaz, P. Kobel, A. de Bosset, and M. Farhat, "Universal scaling law for jets of collapsing bubbles," Phys. Rev. Lett. **107**(20), 204501 (2011).